

PV Panel Performance Evaluation via Accurate V–I Polynomial With Efficient Computation

Hitesh K. Mehta  and Ashish K. Panchal , Member, IEEE

Abstract—For photovoltaic (PV) systems, the perturb-and-observe (P&O) and incremental conductance are the popular peak power tracking (PPT) algorithms. However, their limitations for some PV operating conditions evolves the model based PPT (MBPPT) algorithms. The PV electrical circuit- and mathematical model-based algorithms have been intensively investigated. But, their lengthy computations and requirements of irradiance (G) and temperature (T) sensors increase the cost of on-line implementations. Here, the algorithm (simple and independent of G/T measurements) involves a measurement of three points on the current-voltage (V - I) curve, followed by direct peak power estimation using a simple explicit polynomial V - I model, which is named as a three-point model driven PPT (3MPPT). A different power computation approach makes the PV system to deliver peak power in uniform and partial shading conditions (PSC). Through several numerical simulations in MATLAB/Simulink toolbox, the 3MPPT algorithm is validated and compared with other algorithms. The results feature the improved tracking time and efficiency. An experimental prototype design also confirms the validity of the proposed algorithm. The 3MPPT has superior performance than the P&O in full and half irradiance as well as in PSC.

Index Terms—Maximum power point tracking (MPPT), model-based MPPT, photovoltaics (PVs), single-diode-model (SDM), uniform and partial shading conditions.

I. INTRODUCTION

PHOTOVOLTAIC (PV) power being highly dependent on the solar irradiance (G) and ambient temperature (T), the PV module's peak power tracking (PPT) is only made possible via a converter control algorithm. Two most popular algorithms, the perturb-and-observe (P&O) and the incremental conductance perform the task by sensing and perturbing the module's voltage (V) and current (I) without any need for the G and T measurements [1], thus the power processing becomes cost-effective. However, their shortcomings are: steady-state power oscillations; power losses; and less power transfer due to drift away in case of rapid change in G [2]. These issues can be

Manuscript received August 5, 2021; revised September 16, 2021; accepted September 20, 2021. Date of publication October 11, 2021; date of current version October 21, 2021. (Corresponding author: Ashish K. Panchal.)

Hitesh K. Mehta is with the Department of Electrical Engineering, Sardar Vallabhbhai National Institute of Technology, Surat 395007, India (e-mail: hitesh.mehta@scet.ac.in).

Ashish K. Panchal is with the Department of Electrical Engineering, Sardar Vallabhbhai National Institute of Technology, Surat 395007, India (e-mail: akp@eed.svnit.ac.in).

Color versions of one or more figures in this article are available at <https://doi.org/10.1109/JPHOTOV.2021.3115250>.

Digital Object Identifier 10.1109/JPHOTOV.2021.3115250

overcome by adopting zero-oscillation and drift-free algorithms [3]. Further, the trade-off between accuracy and convergence speed can be mitigated by selecting variable step-size perturbations. A step-size, dependent on nonlinear PV curve, can be optimized by the artificial intelligence techniques such as fuzzy logic [4], neural network [5] and genetic algorithm [6].

These algorithms have shown remarkable improvements in the PV performance with uniform irradiance. Nonetheless, for a PV system with the partial shading conditions (PSC), these algorithms are not fit for the global PPT (GPPT) due to multiple peaks in the voltage-power (V - P) curve [7]. On the contrary, the nature-inspired and stochastic optimization algorithms provide an accurate solution with rapid tracking time by skipping the local peaks in the V - P curve. Many algorithms have been tested for the PV system with PSC, viz. the fusion firefly algorithm [8], chaotic flower pollination algorithm [9], enhanced whale optimization algorithm [10], teaching learning based optimization [11], wind driven optimization [12], etc.

Somewhat different PV-PPT algorithms, known as model-based PPT (MBPPT) [13]–[14], compute V - I curve, and set the PV operation to the voltage at the peak power without tracking. Moreover, they provide oscillations-free steady-state and smooth dynamic operations. Algorithms based on the PV electrical circuit using single-diode-model (SDM) have been reported in the literatures. Cristaldi *et al.* [15] used a simple PV series-circuit with an open-circuit voltage source, a diode and a resistance. Mahmoud and El-Saadany [16] converted an implicit circuit model into an explicit one by replacing the series resistance drop with a voltage dependent source. Mahmoud [17] used the SDM circuit with only shunt resistance, and provided an explicit expression for the voltage at peak power. Similarly, Batzelis [18] used the SDM, and derived explicit expressions to directly compute V and I at the peak power in terms of the five parameters using the Lambert W function. In general, the circuit model driven algorithms need the knowledge of five parameters in *a priori* (mostly derived from the datasheet information) [15]–[18], additional computation burden to evaluate extra model parameters [16], and the G/T measurements. The G and T measurements require sensors and increase the implementation cost. However, G is computed online in [15], similarly T in [16] and both in [19].

In order to avoid the above mentioned necessities by the circuit MBPPT algorithms, alternately, the polynomial models have been used. The polynomial expresses an explicit relation between V - I or V - P . The polynomial coefficients are computed

online using the analytical/curve fitting techniques by measuring a few (V , I) coordinates, followed by the voltage estimation at peak power. Thus, the algorithm is independent of the five parameters and the G/T requirements. For example, Blanes *et al.* [20] used the sixth order $V-I$ polynomial, and [21] used the quadratic $V-P$ polynomial. Cristaldi *et al.* [22] proposed a new expression for V at the peak power as a function of I and T . However, the offline computation of the polynomial coefficients and T measurement requirements are the drawbacks.

One more explicit $V-I$ polynomial existed in [23], [24] with only three coefficients, and requires three (V , I) coordinates [short-circuit (SC), open-circuit (OC), and peak power points] to obtain the SDM five parameters and the full curve. Therefore, it is named as the three-point model (3PM). Using simulations in [25], the 3PM is extensively explored to study the PV module's behavior with variations in G and T as well as in PSC. Patel *et al.* [26] provided an explicit formula for V at the peak power using the 3PM in the STC. However, the use of 3PM for real-time PV-PPT, poses difficulties in the curve identification and the peak power estimation, because of the frequent SC, OC, and peak power points measurements. This problem is overcome in [27] by measuring any three (V , I) coordinates in neighborhood of the peak power. Though the algorithm provides the explicit determination of the peak power, the accuracy is highly dependent on the precise values of the 3PM coefficients. However, the precise values are decided by appropriate locations of the three coordinates in neighborhood of the peak power. Thus, the peak power computation is direct but the model identification is based on trial-and-error adjustment of the coordinates. In contrast to the previous concept, this article proposes a better way of the 3PM coefficients' identification which is totally independent of three coordinates' locations. Further, any coordinates' locations guarantee stable model convergence and provide highest accuracy in the peak power estimation (illustrated later). Although, the algorithm in [27] is tested on a small power application through a single PV module-battery charging system operating under uniform irradiance, its use is not extended for large PV power applications working under PSC, which is also addressed here.

The rest of this article is organized as follows. Section II includes the main contributions of the proposed article. Section III represents the derivation of the 3PM from the SDM, the MPP computation from the 3PM, the 3PM coefficients computation and the proposed algorithm in uniform and partial shading conditions. Section IV illustrates the simulation studies of the 3MPPT algorithm, wherein the results of the PV systems are presented in uniform and partial shading conditions. Also, the results comparison with other algorithms is presented. Section V describes the experimental details and the results obtained by the 3MPPT and P&O algorithms in uniform and partial shading conditions. Finally, Section VI concludes this article.

II. MAIN CONTRIBUTIONS

The contents explain the derivation of the 3PM from the SDM; the derivation of explicit formula to directly evaluate V at the peak power in terms of the 3PM; the computation the

3PM coefficients and PV-PPT mechanism in uniform irradiance and in PSC; the accuracy analysis by the 3PM proposed in [27] and the article; the assessment of the 3MPPT for a PV module/a PV array in uniform irradiance and in PSC through several simulation studies and the comparison with other five algorithms; and the experimental assessment of the 3MPPT in uniform irradiance and in PSC together with its comparison to the P&O.

III. 3MPPT ALGORITHM

A. Derivation for 3PM From SDM (Appendix-A)

For a PV module, the well-known SDM $V-I$ equation based on practical circuit is given as

$$I = I_L - I_0 \left\{ \exp \left(\frac{V + IR_s}{V_t} \right) - 1 \right\} - \frac{V + IR_s}{R_{sh}} \quad (1)$$

where I_L = light current, I_0 = reverse saturation current, n = ideality factor, R_s = series resistance, R_{sh} = shunt resistance, q = electron charge, k = Boltzmann constant, $V_t = nkT/q$ = thermal voltage, and T = cell temperature in K . The datasheet information (the SC current I_{SC} and the OC voltage V_{OC}) and the valid assumption for a PV module ($\exp\{(V_{OC} - I_{SC}R_s)/V_t\} \gg 1$) [28] transfer (1) into the following expression:

$$I = I_{SC} - \left\{ \frac{V}{R_{sh} + R_s} \right\} - \left\{ I_{SC} - \frac{V_{OC}}{R_{sh} + R_s} \right\} \times \exp \left\{ \frac{V - V_{OC} + IR_s}{V_t} \right\}. \quad (2)$$

With high R_{sh} (500–1000 Ω) for the silicon modules, the assumptions, $I_{SC} \gg V/(R_{sh} + R_s)$ and $I_{SC} \gg V_{OC}/(R_{sh} + R_s)$, in (2) are valid. Further, on the right-hand side of (2), the term IR_s can be neglected in comparison with $(V - V_{OC})$ and (2) is rearranged as

$$I = I_{SC} - I_{SC} \left\{ \exp \left(\frac{V}{V_{OC}} - 1 \right) \right\}^{\left(\frac{V_{OC}}{V_t} \right)}. \quad (3)$$

For a module, the condition $-1 < (V/V_{OC}) - 1 < 0$ is always true. Therefore, $\exp\{(V/V_{OC}) - 1\} \approx 1 + (V/V_{OC}) - 1$, approximation is also valid in (3). Thus, (3) is simplified as

$$I = I_{SC} - I_{SC} \left(\frac{V}{V_{OC}} \right)^{\left(\frac{V_{OC}}{V_t} \right)}. \quad (4)$$

Equation (4) can be also rearranged into following form:

$$I = I_{SC} - \frac{I_{SC}}{\left(\frac{V_{OC}}{V_t} \right)} V^{\left(\frac{V_{OC}}{V_t} \right)}. \quad (5)$$

Therefore, (5) is represented in a simple polynomial model as

$$I = c + aV^b \quad (6)$$

where a , b , and c are the model coefficients. The coefficients change with variations in the PV operating conditions G and T . Equation (6) represents an explicit expression for the $V-I$ curve and the three coefficients can be computed on-line via three (V , I) coordinates measurements. Hence, (6) is defined as the 3PM.

B. Derivation for Voltage at Peak Power From 3PM

The peak power position (V_{PP} , I_{PP}) on V - I curve can be set as

$$\frac{dI}{dV} = -\frac{I_{PP}}{V_{PP}}. \quad (7)$$

Therefore, the condition in (7) is also applicable to the V - I curve in (6). Equation (6) is differentiated with respect to V , and is written at the peak power using the following equation:

$$\frac{dI}{dV} = abV_{PP}^{b-1}. \quad (8)$$

Equating (7) and (8), the following expression is yielded

$$abV_{PP}^{b-1} = -\frac{I_{PP}}{V_{PP}}. \quad (9)$$

As the V - I curve must pass through (V_{PP} , I_{PP}), (6) can be expressed as

$$I_{PP} = c + aV_{PP}^b. \quad (10)$$

Substituting (10) into (9), the following explicit expression is defined for V at the peak power

$$V_{PP} = \left(-\frac{c}{a} \times \frac{1}{1+b} \right)^{\frac{1}{b}}. \quad (11)$$

Equation (11) is derived from the 3PM in (6), is to be used for the PPT, and henceforth is referred as the 3MPPT. The obtained V_{PP} value acts as a reference signal to decide the duty ratio for a boost converter.

C. Computation for 3PM Coefficients (Appendix-B)

When the PV operating conditions G and T change, the proposed algorithm initiates to identify new values of the coefficients by three (V , I) coordinates (without the G and T measurements!). The peak power coordinates (V_{PP} , I_{PP}) before the change are set equal to (V_2 , I_2), and two more coordinates (V_1 , I_1) and (V_3 , I_3) are measured in neighborhood to (V_2 , I_2). Since the coordinates have to satisfy the new V - I curve, the substitution of three coordinates into (6), and further simplifications in the resulted equations give the following nonlinear expression for the b coefficient:

$$\left(\frac{V_1}{V_2} \right)^b + \left(\frac{I_1 - I_2}{I_2 - I_3} \right) \left(\frac{V_3}{V_2} \right)^b - \left(\frac{I_1 - I_2}{I_2 - I_3} \right) - 1 = 0. \quad (12)$$

First, the b coefficient is solved iteratively using Newton-Raphson method. Subsequently, the other coefficients are solved using (13) and (14) as following:

$$a = \left(\frac{I_2 - I_3}{V_2^b - V_3^b} \right) \quad (13)$$

$$c = I_1 - aV_1^b. \quad (14)$$

D. 3MPPT Algorithm for a PV System With Uniform Irradiance and PSC

For the uniform irradiance conditions, when a change in I (beyond a threshold) is sensed due to a variation in G , the

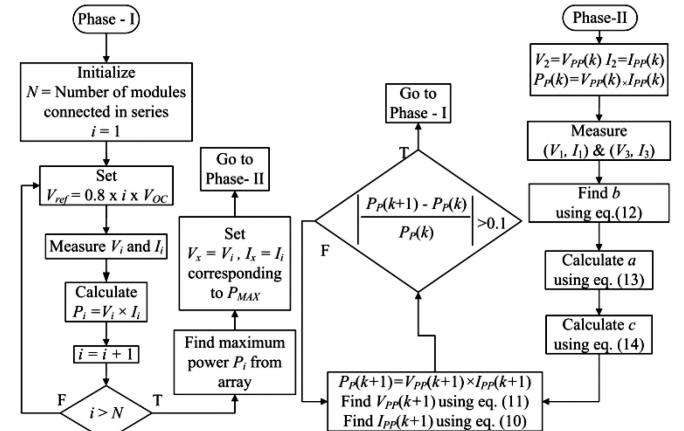


Fig. 1. 3MPPT flow-chart for uniform irradiance and PSC.

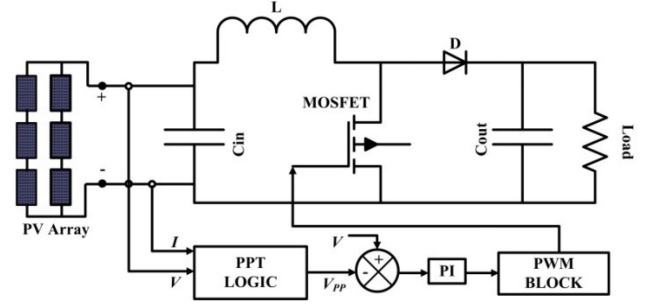


Fig. 2. Schematic block-diagram of the PV system and its control.

algorithm identifies new coefficients and computes new V_{PP} by (11). Only phase-II is in action for such operational changes as presented in Fig. 1. The algorithm also checks the change in the normalized peak power ΔP_P at the end of iteration, if the change is beyond the threshold (0.1 here), the PSC is detected [29]. Then, the algorithm enters in phase-I as shown in Fig. 1. The phase-I fixes the global peak power (GPP) position by scanning the V - P curve in larger steps. The power at $0.8 \times i \times V_{OC}$ (where $i = 1, 2, 3, \dots, N$ (= number of series connected modules)) is checked by deliberately changing the converter duty ratio in larger steps. The maximum power of N steps is the GPP position and then algorithm activates again phase-II to compute accurate GPP. Thus, both phase-I and -II decide the operation in PSC.

IV. SIMULATION RESULTS

Fig. 2 represents the PV system with a PV module/a PV array, a boost converter and a resistive load. The Appendix-C and D contains the 60 W PV module specifications and the boost converter design parameters, respectively. The complete system and its control are developed in MATLAB/SIMULINK toolbox. The simulation studies are as follows.

To prove the model accuracy and convergence stability irrespective of the three coordinate's locations, a comparison is studied between the computation methods in the article and proposed in [27].

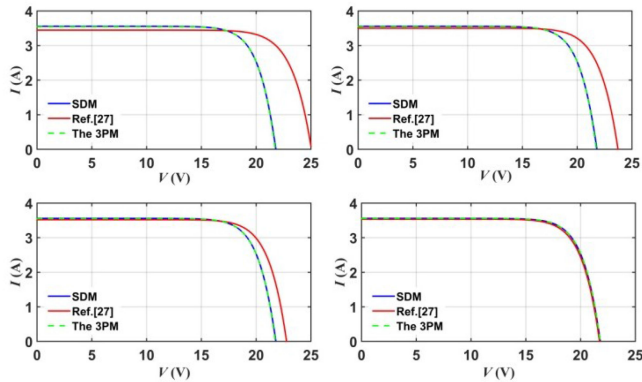


Fig. 3. V - I curves for the coordinates' selection $\pm 5\%$ (T-L), $\pm 10\%$ (T-R), $\pm 15\%$ (B-L), and $\pm 20\%$ (B-R) in neighborhood of the peak power with (T-top, M-middle, B-bottom, L-left, and R-right).

In the uniform irradiance, the 3PMPPT algorithm performance is assessed in steady-state and dynamic conditions. The performance is also compared with the other algorithms such as, the P&O, in [15], [17], [18], and [22]. Proposed algorithm is tested for a 10×10 PV array subjected to PSC.

A. Comparison of Three Coordinates Selection

In [27], three coordinates (V_1, I_1) , (V_2, I_2) , and (V_3, I_3) selection has to satisfy two conditions: the coordinates are selected such that $I_1 > I_2 > I_3$, $V_1 < V_2 < V_3$, and $V_{12} < V_{23}$, and the model coefficients are computed such that $\alpha (= c) > 0$, $\beta (= a) < 0$, and $\gamma (= b) > 1$. If both the conditions are not satisfied then the selection process is repeated till the conditions are satisfied. In short, though the PPT algorithm claims to have explicit determination of the model coefficients, the selection of the three coordinates is still iterative, and thus the entire peak power estimation is an iterative process.

In this article, it is worth noting that the three coordinate's selection has no condition. Fig. 3 illustrates the full V - I curves obtained for different coordinate's selections, i.e., $\pm 5\%$, $\pm 10\%$, $\pm 15\%$, and $\pm 20\%$ in the neighbourhood to V_{PP} . The curves are estimated by the SDM, methods in [27] and in this article for the four modules under STC. The curves by the present method (dotted green line) are in good agreement with those by the SDM (blue line) for all four selections. However, the curves by the method in [27] (red line) have large deviations with respect to the curves by the SDM for the first three selections [see Fig. 3 (T-L), (T-R), and (B-L)], because the selection criteria are not met. Interestingly, a good agreement between the two curves for the last selection [see Fig. 3 (B-R)] is as a result of perfect condition match. This fact is further confirmed by very small root-mean-squared-error (RMSE) in the currents and very small deviation in the peak power by the present method than in [27] given in Table I. The stable model convergence by the present method is credited to the appropriate initial guess for the b coefficient. From (5) and (6) $b_0 = V_{OC}/V_t$, which can be easily calculated at the STC from the datasheet. Thus, though the b coefficient computation is iterative in this method, the V - I curve and the peak power estimation are accurate for any

TABLE I
COMPARISON IN RMSE AND ERROR IN PEAK POWER OBTAINED BY THE MODEL IN [27] AND THE 3PM FOR DIFFERENT PV MODULES

PV Module	V_1, V_3 % away from V_2	Model in Ref. [27]		3PM model	
		RMSE	Error P_p (%)	RMSE	Error P_p (%)
60 W	± 5	0.5481	-11.5774	0.0151	-0.0006
	± 10	0.4551	-7.1661	0.0150	-0.0020
	± 15	0.3059	-3.3144	0.0117	-0.0025
	± 20	0.0468	1.5446	0.0085	-0.0019
160 W	± 5	0.8796	-19.9804	0.0367	-0.0001
	± 10	0.8506	-16.7015	0.0345	0.0000
	± 15	0.7005	-9.3249	0.0231	-0.0005
	± 20	0.6227	-7.4391	0.0136	0.0000
200 W	± 5	1.5187	-17.1088	0.3725	-0.0001
	± 10	1.4296	-13.9966	0.3092	-0.0006
	± 15	1.2518	-10.1162	0.2129	-0.0034
	± 20	0.9525	-5.7909	0.0971	-0.0136
250 W	± 5	1.5590	-17.9982	0.0848	-0.0001
	± 10	1.4860	-14.5698	0.0774	-0.0003
	± 15	1.3055	-10.1082	0.0566	-0.0003
	± 20	0.9615	-5.3501	0.0272	0.0000

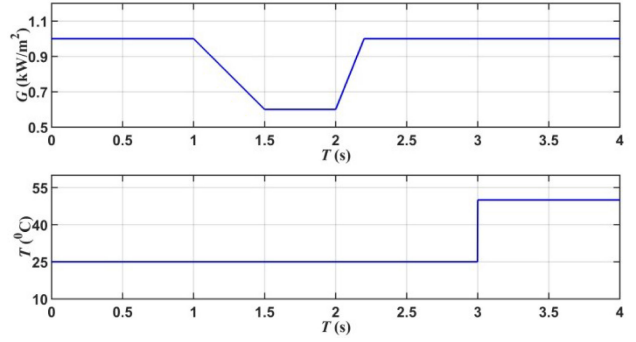


Fig. 4. G and T variations used for the simulation study.

coordinate's selection. Therefore, the present model estimation method is believed to be more powerful than in [27] in any PV operating condition.

B. 3PMPPT for PV Operation in Uniform Irradiance

The PV system is simulated for 4 s with different G and T changes as depicted in Fig. 4. The simulated PV signals shown in Fig. 5 indicate that all the algorithms detect the change and force the PV system to follow, where the highest oscillations by the P&O are clearly observed. The starting tracking time in Table II is 23.5 ms for the 3PMPPT, algorithms in [17] and [22], 33.5 ms for algorithms in [15] and [18], and 185 ms for the P&O. The reasons can be explained as; the first three have direct V_{PP} computation formula and takes least time. Cristaldi *et al.* [15] needs additional G computation, and Batzelis [18] solves using the Lambert W function which is 2.8 to 4.1 times slower than the exponential function in MATLAB [30]. Against all the MBPPT algorithms, the P&O reaches to the peak power in fixed steps and takes the highest time.

As previously mentioned, the algorithm initiates to measure two voltage points (V_1 and V_3) around the V_{PP} ($= V_2$) whenever a change is detected. During the instants, viz. 0.1 s, 1.5 s, 2.2 s

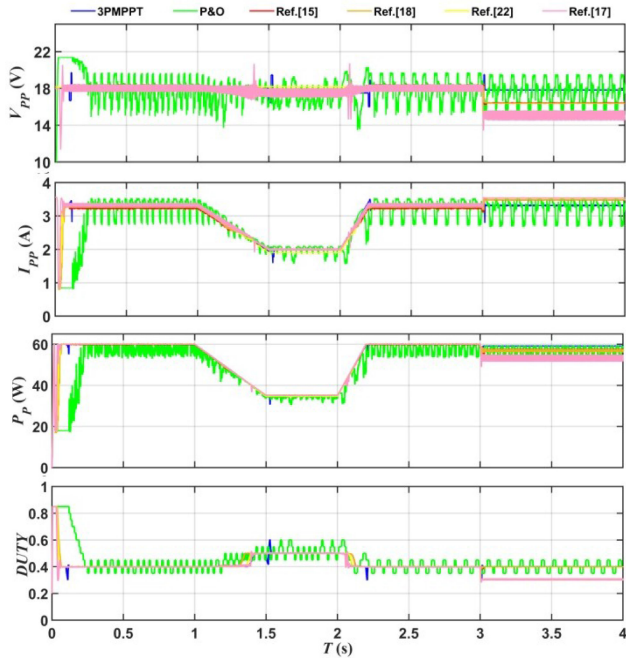
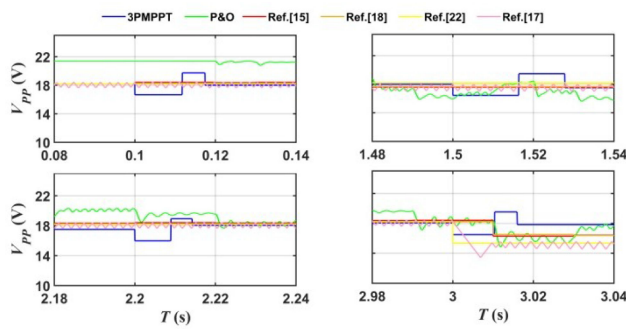


Fig. 5. Simulation results of different PV signals in uniform irradiance.

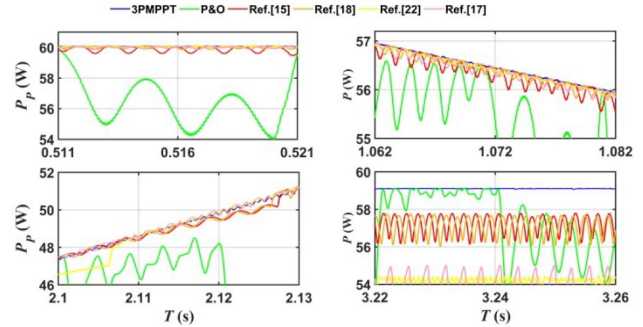
TABLE II
PERFORMANCE COMPARISON OF VARIOUS PPT ALGORITHMS

Methods	Oscillations	Start Time (ms)	G and T Meas. Required/Sensors*	Tracked Power (W)	Static Efficiency (%)	Dynamic Efficiency (%)
P&O	Large	185	No /2	60.1	94.8	68.42
Ref. [15]	Medium	33.5	G and T/4	60.08	98.5	98.32
Ref. [18]	Medium	33.5	T/3	60.09	98.64	98.46
Ref. [17]	Small	24	T/3	60.09	98.7	97.8
Ref. [22]	Small	23.5	T/3	60.1	99.5	98.85
3PMPPPT	No	23.5	No/2	60.1	99.95	98.83

*All algorithms require two sensors for V and I measurements. Additional sensors are required for the G/T measurements. The 3PMPPPT algorithm is independent of the G/T measurements like the P&O and needs only two sensors. On the other hand, the other algorithms require more than two sensors.

Fig. 6. V_{PP} zoom views at 0.1 s (T-L), 1.5 s (T-R), 2.2 s (B-L), and 3 s (B-R).

(change in G), and 3 s (change in T), the PV voltage actions are depicted in Fig. 6. In all the subplots, the two-step changes in the blue line indicate the V_1 and V_3 measurements by the 3PMPPPT. All the MBPPT algorithms settle the voltage near to 18 V whereas much deviated by the P&O at the instants of the

Fig. 7. P_P zoom views during steady-state (T-L and B-R) and dynamic (T-R and B-L) conditions.

change in G . Note, all the MBPPT algorithms compute V_{PP} , and the P&O delays the PPT with the continuous perturbation in the voltage. Interestingly, after the change in T , the 3PMPPPT and P&O settle to 17.3 V, whereas a small deviation in the voltage is observed by the other MBPPT algorithms. The previous both algorithms track the peak power using only the (V, I) coordinates without the T measurements and the MBPPT algorithms need that.

Fig. 7 (T-L) and (B-R) illustrates the steady-state conditions mentioning oscillations-free operation by the 3PMPPPT, minimum oscillations by [17] and [22], a little larger oscillation by [15] and [18], and the highest oscillations by the P&O. As a result, the tracking efficiencies in steady-state and dynamic conditions also appear in that sequence as given in Table II as per EN50530 test conditions. The highest is for the 3PMPPPT and the lowest for the P&O. All MBPPT algorithms perform with the tracking efficiency $>98\%$ except the P&O with 94.8% which is caused by delayed tracking. Fig. 7 (T-R) and (B-L) indicates the variation in the power during the dynamic change in the operating conditions. Once again, the performance by the 3PMPPPT, [17] and [22] with smooth change; by [15] and [18] with little larger oscillations; and by the P&O the highest oscillations are observed.

Concluding the comparisons, the present algorithm has the similar performance as in [17] and [22] owing to direct V_{PP} computation. However, the difference between the 3PMPPPT and other two is the power tracking without the G and T measurements as in the P&O as given in Table II. Next in the sequence, the algorithms in [15] and [18] offer a little less performance in comparison with the previous three, as the later two have additional computation burden and the T measurement. Overall, when the efficient and fast power tracking, as well as the simplicity like the P&O, are needed the 3PMPPPT algorithm is recommended.

C. 3PMPPPT for PV Operation in PSC

When a 10×10 PV array is operating under PSC with different four irradiance levels shown in Fig. 8(L), the system has four peaks in its $V-P$ curve exhibiting the GPP 3023 W at 146.1 V [see Fig. 8(R)]. It can be observed in Fig. 9, the PV voltage (V_{PP}) changes in ten steps (corresponding to ten modules in a PV string) between 0 to 0.1 s, which is attributed

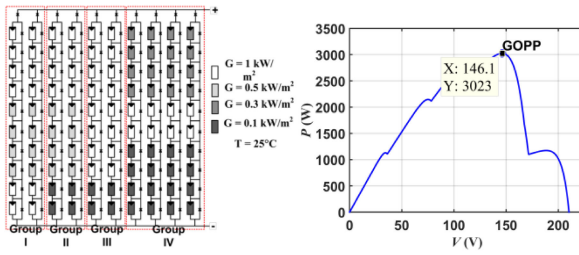
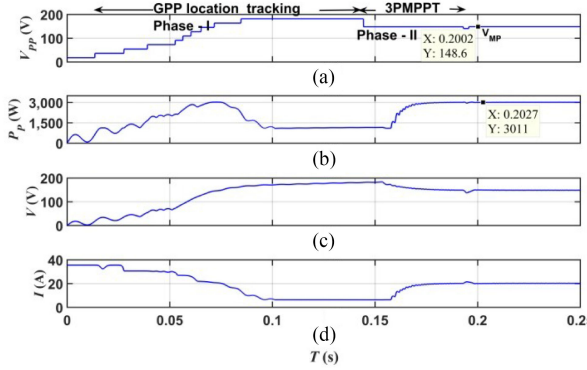
Fig. 8. 10×10 PV array (L) and its V - P curve (R).

Fig. 9. Simulation results of different PV signals in PSC.

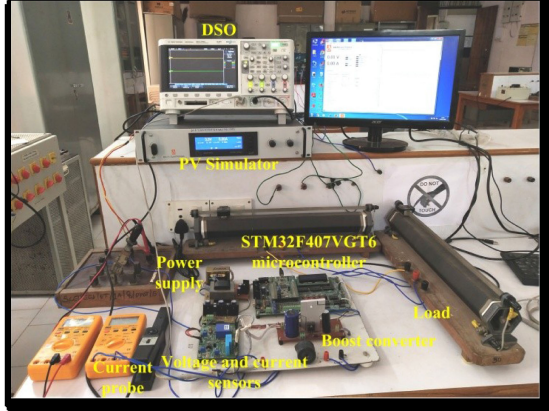


Fig. 10. Experimental setup with power-circuit, control-circuit, and display.

to the GPP position tracking in the phase-I. After 0.1 s, a two-step change observed in V_{pp} shows two coordinates' measurements followed by the true GPP computations as shown in the phase-II. Finally, the system settles at 148.6 V with the GPP 3011 W. Thus, the 3PMPPPT shows an error 0.4% in the GPP and 1.7% in the associated V_{in} in comparison with the SDM. These little deviations are caused due to the approximation in the 3PM than the SDM. Therefore, the 3PMPPPT algorithm has proven its capability for the GPPT in PSC.

V. EXPERIMENTAL RESULTS

Fig. 10 displays the photograph for the experimental setup. The PV simulator (make DELTATEK), via a boost converter, is connected to a resistive load (125Ω). The PV simulator provides the 60 W module characteristic. The PV-PPT algorithms (the 3PMPPPT and P&O) are implemented in an industrial

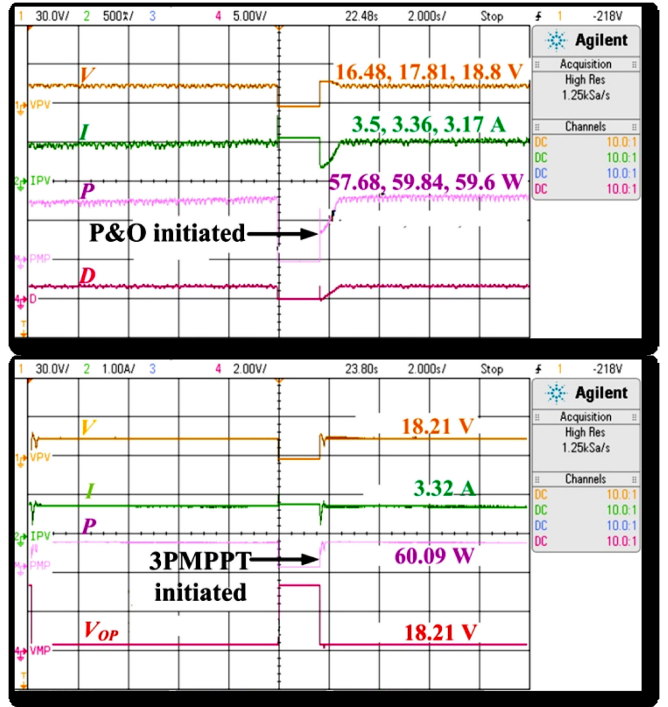
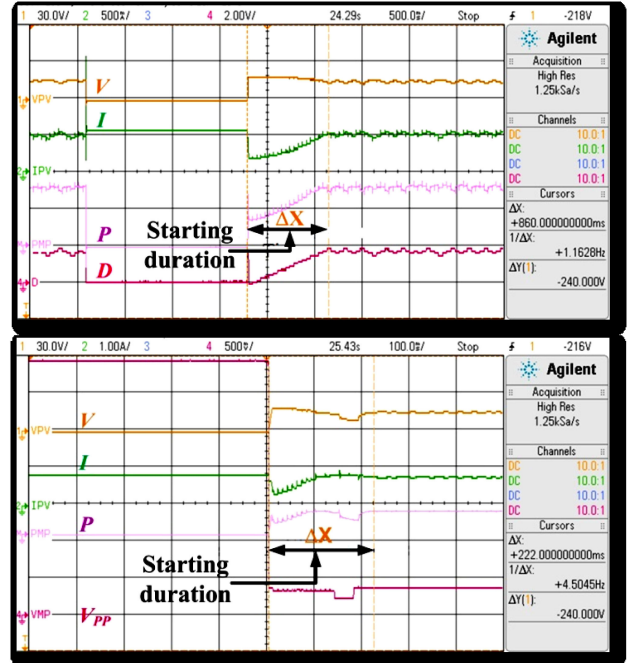
Fig. 11. DSO snapshots for (T) P&O and (B) 3PMPPPT at 1 kW/m^2 .

Fig. 12. Zoom views for (T) P&O and (B) 3PMPPPT at the starting instant.

standard microcontroller (STM32F407VGT6). The PV signals (V and I) are measured using hall-effect sensors (calibrated for 100 V and 10 A) which also provide an isolation between the power and control circuits. The measurement noise is filtered out by a conditioner circuit. Then, the V and I signals (each 3 V) are fed to the microcontroller ADC channels. Note, the Adc samples the signals every 10 ms to initiate the control action.

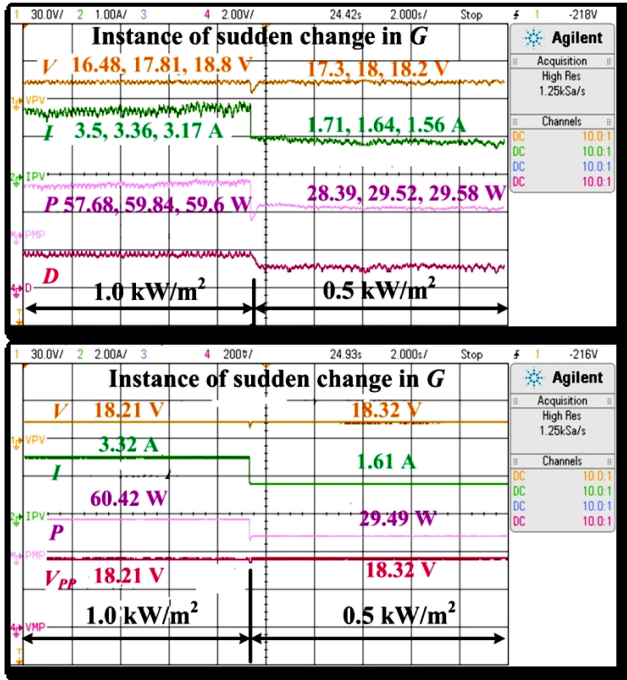


Fig. 13. DSO snapshots for (T) P&O and (B) 3PMPPPT with sudden change in G .

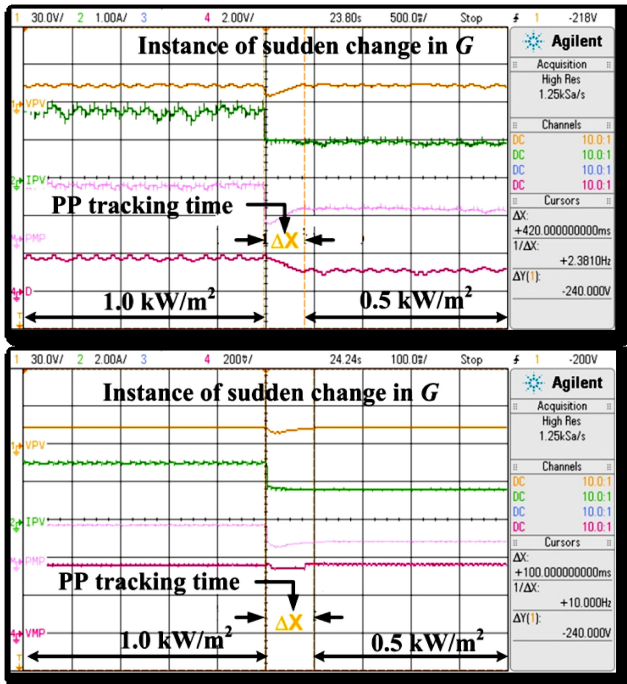


Fig. 14. Zoom views for (T) P&O and (B) 3PMPPPT at the instant change in G .

A. 3PMPPPT for PV Operation in Uniform Irradiance

Different PV signals shown in the DSO snapshots in Fig. 11 compare the 3PMPPPT and P&O. The steady-state power oscillations [see Fig. 11(T)] are observed with three steps around 60 W, i.e., 57.68, 59.84, and 59.6 by the P&O. However, the

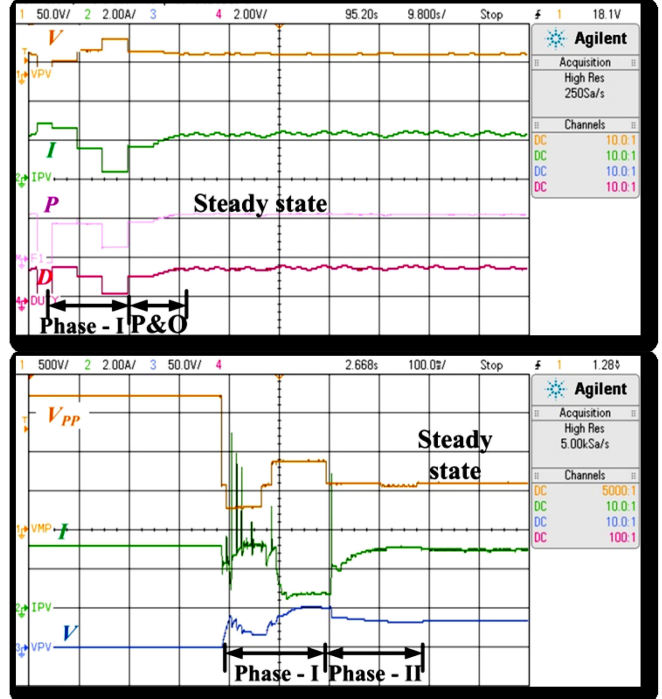


Fig. 15. 3 × 2 PV array on the roof-top of the institute (T), DSO snapshots of P&O (M), and 3PMPPPT (B).

3PMPPPT delivers constant power 60.09 W [see Fig. 11(B)]. Observing the zoom views during starting in Fig. 12(T) and (B), the P&O tracks the power in fixed steps within 860 ms, whereas the proposed algorithm detects three coordinates, computes V_{PP} and tracks the power within 222 ms. Thus, the 3PMPPPT performs fast tracking with the oscillations-free operations over the P&O.

With a sudden irradiance change from 1 to 0.5 kW/m², the P&O changes the power to half with three steps oscillations [see Fig. 13(T)], whereas the 3PMPPPT reduces the PV current from 3.32 to 1.61 A (half current) and delivers half power [see Fig. 13(B)]. Finally, the 3PMPPPT completes the task within 100 ms whereas the P&O takes 420 ms, as indicated in Fig. 14(T) and (B). Therefore, again the proposed algorithm offers its superior performance than the P&O in sudden irradiance change.

B. 3PMPPPT for PV Operation in PSC

The algorithms are also tested on a 3 × 2 PV array under PSC operating in the real environmental conditions located on the roof-top of the institute. As shown in the photograph in

Fig. 15(T), one of the modules of a string is completely shaded by a card-board. The proposed and P&O algorithms fix the location for the GPP in the phase-I as marked in Fig. 15(M) and (B). Thereafter, a distinct difference appears in both algorithms to reach the exact GPP. The P&O tracks the power in fixed steps, and maintains the steady-state oscillations, whereas the 3PMPPPT computes the exact GPP using the phase-II and performs with no oscillations.

VI. CONCLUSION

Using the SDM together with a few valid assumptions, the 3PM is derived, which leads to an explicit expression for V_{PP} as a function of the model coefficients. The 3PMPPPT algorithm identifies the change in operating conditions, computes V_{PP} by an online measurement of three coordinates in uniform irradiance. It automatically identifies the PSC, and computes an accurate GPP in phase-I and -II.

The simulation results summarize that the present method has provided stable and accurate 3PM identification than the existed one, and the process is irrespective of the three coordinates' locations near to the peak power. The 3PMPPPT works efficiently with minimum tracking time in comparison with the other algorithms in uniform irradiance. It successfully identifies and tracks the GPP for a large PV array.

The experimental results establish that the 3PMPPPT performs rapidly and oscillations-free in comparison with P&O when the 60 W module irradiance drops from 1 kW/m² to half. It performs better than P&O in case of an on-site 3 × 2 PV array when artificially shaded.

The limitations of proposed 3PMPPPT algorithm are, it is model based algorithm and requires the Newton-Raphson iterative method to solve for the b coefficient. Therefore the NR method has to be implemented in the microcontroller. Since the 3PM is approximated from the SDM, the 3PMPPPT estimates a little deviated power for a large PV system operating in PSC.

APPENDIX

A) Complete Derivation of the 3PM: The conditions I_{SC} and V_{OC} substitution in the SDM in (1) result in following expressions:

$$\left(1 + \frac{R_s}{R_{sh}}\right) I_{SC} = I_L - I_0 \left(\exp\left(\frac{I_{SC} R_s}{V_t}\right) - 1 \right) \quad (S1)$$

$$0 = I_L - I_0 \left(\exp\left(\frac{V_{OC}}{V_t}\right) - 1 \right) - \frac{V_{OC}}{R_{sh}}. \quad (S2)$$

The I_L elimination from (S1) and (S2) yields the following:

$$I_0 = \frac{\left(1 + \frac{R_s}{R_{sh}}\right) I_{SC} - \frac{V_{OC}}{R_{sh}}}{\exp\left(\frac{V_{OC}}{V_t}\right) - \exp\left(\frac{I_{SC} R_s}{V_t}\right)}. \quad (S3)$$

The (S2) and (S3) substitution in (1) generates the following expression:

$$I = I_{SC} - \frac{V}{R_s + R_{sh}} - \left(I_{SC} - \frac{V_{OC}}{R_s + R_{sh}} \right)$$

$$\times \left(\frac{1 - \exp\left(\frac{V + I R_s - I_{SC} R_s}{V_t}\right)}{1 - \exp\left(\frac{V_{OC} - I_{SC} R_s}{V_t}\right)} \right). \quad (S4)$$

On the right hand side in (S4), both the exponential terms $\gg 1$ [28], (S4) can be reorganized as

$$I = I_{SC} - \left\{ \frac{V}{R_{sh} + R_s} \right\} - \left\{ I_{SC} \frac{V_{OC}}{R_{sh} + R_s} \right\} \\ \times \exp\left(\frac{V - V_{OC} + I R_s}{V_t}\right). \quad (S5)$$

With high R_{sh} (500–1000 Ω) for the silicon modules, the assumptions, $I_{SC} \gg V/(R_{sh} + R_s)$ and $I_{SC} \gg V_{OC}/(R_{sh} + R_s)$, in (2) are valid. Further, on the right hand side of (2), the term $I R_s$ can be neglected in comparison with $(V - V_{OC})$ and (2) is rearranged as

$$I = I_{SC} - I_{SC} \left\{ \exp\left(\frac{V}{V_{OC}} - 1\right) \right\}^{\left(\frac{V_{OC}}{V_t}\right)}. \quad (S6)$$

For a module, the condition $-1 < (V/V_{OC}) - 1 < 0$ is always true. Therefore, $\exp\{(V/V_{OC}) - 1\} \approx 1 + (V/V_{OC}) - 1$, approximation is also valid in (S6). Thus, (S6) is simplified as

$$I = I_{SC} - I_{SC} \left(\frac{V}{V_{OC}} \right)^{\left(\frac{V_{OC}}{V_t}\right)}. \quad (S7)$$

Equation (S7) can be also rearranged into following form:

$$I = I_{SC} - \frac{I_{SC}}{V_{OC}^{\left(\frac{V_{OC}}{V_t}\right)}} V^{\left(\frac{V_{OC}}{V_t}\right)}. \quad (S8)$$

Therefore, (S8) is represented in a simple polynomial model as

$$I = c + aV^b \quad (S9)$$

where a , b , and c are the model coefficients.

B) Derivation of the 3PM Coefficient: Assuming the set of three coordinates (V_1, I_1) , (V_2, I_2) and (V_3, I_3) satisfy the 3PM in (6) and can be written as following:

$$I_1 = c + aV_1^b \\ I_2 = c + aV_2^b \\ I_3 = c + aV_3^b. \quad (S10)$$

Three expressions in (S10) can be equated as following:

$$c = I_1 - aV_1^b = I_2 - aV_2^b = I_3 - aV_3^b. \quad (S11)$$

The expressions in (S11) can be further simplified and the following expression for the a coefficient can be written as:

$$aV_2^b - aV_3^b = I_2 - I_3 \Rightarrow a(V_2^b - V_3^b) = I_2 - I_3 \\ \Rightarrow a = \frac{(I_2 - I_3)}{(V_2^b - V_3^b)}. \quad (S12)$$

The coefficient a substitution from (S11) into (S11) generates the following:

$$I_1 = \frac{(I_2 - I_3)}{(V_2^b - V_3^b)} V_1^b + I_2 - \frac{(I_2 - I_3)}{(V_2^b - V_3^b)} V_2^b. \quad (\text{S13})$$

Further simplification in (S13) represents the following expression:

$$\left(\frac{I_1 - I_2}{I_2 - I_3} \right) = \left(\frac{V_1^b - V_2^b}{V_2^b - V_3^b} \right) \Rightarrow \left(\frac{I_1 - I_2}{I_2 - I_3} \right) = \left(\frac{\frac{V_1^b}{V_2^b} - 1}{1 - \frac{V_3^b}{V_2^b}} \right). \quad (\text{S14})$$

Equation (S14) is simplified into the following expression in terms of the b coefficient:

$$\left(\frac{V_1}{V_2} \right)^b - \left(\frac{I_1 - I_2}{I_2 - I_3} \right) \left(\frac{V_3}{V_2} \right)^b - \left(\frac{I_1 - I_2}{I_2 - I_3} \right) - 1 = 0. \quad (\text{S15})$$

Equation (S15) is the same as (12).

C) *The 60 W PV Module (TATA Make TBP1260) Specifications at the STC: $V_{\text{OC}} = 21.8 \text{ V}$; $I_{\text{SC}} = 3.56 \text{ A}$, $V_{\text{PP}} = 18.2 \text{ V}$; $I_{\text{PP}} = 3.3 \text{ A}$; and $P_P = 60 \text{ W}$.*

D) *The DC-DC Boost Converter Parameters: inductor = 297 μH ; input capacitor = 2000 μF ; output capacitor = 470 μF ; and switching frequency = 10 kHz.*

REFERENCES

- [1] D. Sera, L. M. D., T. Kerekes, S. V. Spatharu, and R. Teodorescu, "On the perturb-and-observe and incremental conductance MPPT methods for PV systems," *IEEE J. Photovolt.*, vol. 3, no. 3, pp. 1070–1078, Jul. 2013.
- [2] A. K. Podder, N. K. Roy, and H. R. Pota, "MPPT methods for solar PV systems: A critical review based on tracking nature," *IET Renewable Power Gener.*, vol. 13, no. 10, pp. 1615–1632, 2019.
- [3] X. Li, Q. Wang, H. Wen, and W. Xiao, "Comprehensive studies on operational principles for maximum power point tracking in photovoltaic systems," *IEEE Access*, vol. 7, pp. 121407–121420, 2019.
- [4] H. Rezk, M. Aly, M. Al-Dhaifallah, and M. Shoyama, "Design and hardware implementation of new adaptive fuzzy logic-based MPPT control method for photovoltaic applications," *IEEE Access*, vol. 7, pp. 106427–106438, 2019.
- [5] S.-A. Touil, N. Boudjedra, A. Boubakir, and K. E. K. Drissi, "A sliding mode control and artificial neural network based MPPT for a direct grid-connected photovoltaic source," *Asian J. Control*, vol. 21, no. 4, pp. 1892–1905, 2019.
- [6] S. Hadji, J.-P. Gaubert, and F. Krim, "Real-time genetic algorithms-based MPPT: Study and comparison (theoretical an experimental) with conventional methods," *Energies*, vol. 11, no. 2, 2018, Art. no. 459.
- [7] B. Lin, L. Wang, and Q. H. Wu, "Maximum power point scanning for PV systems under various partial shading conditions," *IEEE Trans. Sustain. Energy*, vol. 11, no. 4, pp. 2556–2566, Oct. 2020.
- [8] Y.-P. Huang, M.-Y. Huang, and C.-E. Ye, "A fusion firefly algorithm with simplified propagation for photovoltaic MPPT under partial shading conditions," *IEEE Trans. Sustain. Energy*, vol. 11, no. 4, pp. 2641–2652, Oct. 2020.
- [9] D. Youssi, T. S. Babu, D. Allam, V. K. Ramachandaramurthy, and M. B. Etiba, "A novel chaotic flower pollination algorithm for global maximum power point tracking for photovoltaic system under partial shading conditions," *IEEE Access*, vol. 7, pp. 121432–121445, 2019.
- [10] M. H. Qais, H. M. Hasanien, and S. Alghuwainem, "Enhanced whale optimization algorithm for maximum power point tracking of variable-speed wind generators," *Appl. Soft Comput.*, vol. 86, 2020, Art. no. 105937.
- [11] H. Rezk and A. Fathy, "Simulation of global MPPT based on teaching-learning-based optimization technique for partially shaded PV system," *Electr. Eng.*, vol. 99, no. 3, pp. 847–859, 2017.
- [12] O. Abdalla, H. Rezk, and E. M. Ahmed, "Wind driven optimization algorithm based global MPPT for PV system under non-uniform solar irradiance," *Sol. Energy*, vol. 180, pp. 429–444, 2019.
- [13] L. Cristaldi, M. Faifer, M. Rossi, and S. Toscani, "MPPT definition and validation: A new model-based approach," in *Proc. IEEE Int. Instrum. Meas. Technol. Conf.*, 2012, pp. 594–599.
- [14] Y. Mahmoud, M. Abdelwahed, and E. F. El-Saadany, "An enhanced MPPT method combining model-based and heuristic techniques," *IEEE Trans. Sustain. Energy*, vol. 7, no. 2, pp. 576–585, Apr. 2015.
- [15] L. Cristaldi, M. Faifer, M. Rossi, and S. Toscani, "An improved model-based maximum power point tracker for photovoltaic panels," *IEEE Trans. Instrum. Meas.*, vol. 63, no. 1, pp. 63–71, Jan. 2014.
- [16] Y. Mahmoud and E. F. El-Saadany, "A photovoltaic model with reduced computational time," *IEEE Trans. Ind. Electron.*, vol. 62, no. 6, pp. 3534–3544, Jun. 2015.
- [17] Y. Mahmoud, "A model-based MPPT with improved tracking accuracy," in *Proc. 44th Annu. Conf. IEEE Ind. Electron. Soc.*, 2018, pp. 1609–1612.
- [18] E. I. Batzelis, "Simple PV performance equations theoretically well founded on the single-diode model," *IEEE J. Photovolt.*, vol. 7, no. 5, pp. 1400–1409, Sep. 2017.
- [19] J.-H. Teng, W.-H. Huang, T.-A. Hsu, and C.-Y. Wang, "Novel and fast maximum power point tracking for photovoltaic generation," *IEEE Trans. Ind. Electron.*, vol. 63, no. 8, pp. 4955–4966, Aug. 2016.
- [20] J. M. Blanes, F. J. Toledo, S. Montero, and A. Garrigos, "In-site real-time photovoltaic I-V curves and maximum power point estimator," *IEEE Trans. Power Electron.*, vol. 28, no. 3, pp. 1234–1240, Mar. 2013.
- [21] F.-S. Pai and R.-M. Chao, "A new algorithm to photovoltaic power point tracking problems with quadratic maximization," *IEEE Trans. Energy Convers.*, vol. 25, no. 1, pp. 262–264, Mar. 2010.
- [22] L. Cristaldi, M. Faifer, C. Laurano, R. Ottoboni, S. Toscani, and M. Zanoni, "Model-based MPPT parameter optimization for photovoltaic panels," in *Proc. Int. Conf. Clean Electr. Power*, 2019, pp. 534–538.
- [23] L. Liu, W. Liu, X. Zhang, and J. Ingenhoff, "Research on the novel explicit model for photovoltaic IV characteristic of the single diode model under different splitting spectrum," *Results Phys.*, vol. 12, pp. 662–672, 2019.
- [24] V.J. Chin and Z. Salam, "A new three-point-based approach for the parameter extraction of photovoltaic cells," *Appl. energy*, vol. 237, pp. 519–533, 2019.
- [25] H. K. Mehta, T. Nukala, and A. K. Panchal, "A fast computing three point model for PV system in uniform and non-uniform conditions," *J. Renewable Sustain. Energy*, vol. 10, no. 6, 2018, Art. no. 065501.
- [26] S. J. Patel, G. Kumar, A. K. Panchal, and V. Kheraj, "Maximum power point computation using current–voltage data from open and short circuit regions of photovoltaic module: A teaching learning based optimization approach," *J. Renewable Sustain. Energy*, vol. 7, no. 4, 2015, Art. no. 043112.
- [27] M. J. Z. Zadeh and S. H. Fathi, "A new approach for photovoltaic arrays modeling and maximum power point estimation in real operating conditions," *IEEE Trans. Ind. Electron.*, vol. 64, no. 12, pp. 9334–9343, Dec. 2017.
- [28] K.-I. Ishibashi, Y. Kimura, and M. Niwano, "An extensively valid and stable method for derivation of all parameters of a solar cell from a single current–voltage characteristic," *J. Appl. Phys.*, vol. 103, no. 9, 2008, Art. no. 094507.
- [29] J. Ahmed and Z. Salam, "An accurate method for MPPT to detect the partial shading occurrence in a PV system," *IEEE Trans. Ind. Informat.*, vol. 13, no. 5, pp. 2151–2161, Oct. 2017.
- [30] T. Fukushima, "Precise and fast computation of lambert W-functions without transcendental function evaluations," *J. Comput. Appl. Math.*, vol. 244, pp. 77–89, 2013.